

Single-step synthesis of doped TiO₂ stratified thin-films by atmospheric-pressure chemical vapour deposition†

Cite this: *J. Mater. Chem. A*, 2014, 2, 7082

Carlos Sotelo-Vazquez, Raul Quesada-Cabrera,* Jawwad A. Darr and Ivan P. Parkin*

Locally doped TiO₂ thin-films were engineered by pulsed precursor delivery using atmospheric-pressure chemical vapour deposition. To our knowledge, this is the first example of stratified films deposited in this manner. The optical, structural and morphological properties of the films were investigated using absorption spectroscopy, X-ray diffraction and electron microscopy techniques. Nitrogen-doped TiO₂ stratified thin-films were produced as proof that the new technique would work and that the nature and location of nitrogen species within the films could be studied by X-ray photoelectron spectroscopy. The photocatalytic performance of the films was investigated using the photodegradation of a model organic pollutant (stearic acid). The impact of a stratified configuration and the influence of the type of nitrogen species on enhanced photocatalytic activity are discussed.

Received 23rd February 2014
Accepted 24th March 2014

DOI: 10.1039/c4ta00935e

www.rsc.org/MaterialsA

1. Introduction

Titania (TiO₂) thin-films have been used in a wide range of photocatalysis applications, including water and air-cleaning technologies, water-splitting, self-cleaning materials and degradation of cancer cells and viruses.^{1–4} This is due to its high efficiency in the UV range, chemical inertness, mechanical robustness and relatively low cost.^{4,5} In the last decade, strenuous efforts have been devoted to broaden the photoresponse of TiO₂ into the visible range for solar photocatalysis applications. Some of these approaches include the design of TiO₂-based composite materials,^{6–8} the modification of TiO₂ using dye sensitizers⁹ and the incorporation of metal or non-metal ions into the TiO₂ structure.^{10–16} An interesting strategy, particularly adopted in recent years, is the selective incorporation of dopants (local doping) into semiconductor photocatalyst materials.^{17–20} Local doping typically allows control over structural defects and contributes to a better understanding of the physicochemical properties of the doped materials and their effect on photoactivity. Regardless of the potential benefits of ion-doping in terms of band-structure and electronic-properties, the indiscriminate addition of dopants into TiO₂ host materials, may have a drastic impact on physical properties (crystallinity, morphology, *etc.*), thus affecting their photocatalytic performance. This has certainly been the case in the synthesis of doped semiconductor films *via* chemical vapour deposition (CVD).^{1,21}

A local doping approach in the synthesis of films using CVD may not only minimise any structural impairment in the material but also produce systems with similar properties to those synthesised *via* atomic layer deposition (ALD). ALD is widely used to produce nanostructured thin-films with controlled thickness and crystallinity²² facilitating the engineering of stratified films containing buffer layers for a facile and rapid separation of charge carriers for solar cell applications. This is the case of nanostructured TiO₂ shells²³ and ZnO–TiO₂ films,^{24,25} where recombination of photogenerated carriers on ZnO are quenched by ultrathin TiO₂ layers, improving the efficiency of solar cell devices.

The selective incorporation of dopants into TiO₂ films can be easily achieved by pulsed precursor delivery using CVD. This method involves the introduction of the dopant precursor only during intermittent periods of total deposition time. In the current work, anatase stratified nitrogen-doped TiO₂ films were synthesised in this manner. This is, to the best of our knowledge, the first example of stratified doped photocatalytic thin-films synthesised by CVD. It is different to ALD because the process does not rely on monolayer coverage and subsequent chemical reaction. In this work we found that despite the high nitrogen content of the locally doped regions in the stratified films, their overall crystallinity was apparently unaffected in the doping process, as evidenced by X-ray diffraction. This allowed a fair comparison among similar undoped, non-stratified and stratified samples and correlation between the nature and concentration of the dopant and their influence on photocatalytic activities during degradation of a model organic pollutant. The enhanced activity of stratified N-TiO₂ films will be discussed. Nitrogen was chosen here as a model dopant, since N-doped TiO₂ materials have been extensively

University College London, Dept. Chemistry, Christopher-Ingold Laboratories, 20 Gordon St., London, WC1H 0AJ, UK. E-mail: r.quesada@ucl.ac.uk; i.p.parkin@ucl.ac.uk; Fax: +44 (0)20 7679 7463; Tel: +44 (0)20 7679 4669

† Electronic supplementary information (ESI) available. See DOI: 10.1039/c4ta00935e

investigated, however, the local doping approach can be easily applied to any dopant or mixtures of co-dopants and it represents a promising new strategy in the design and development of a new generation of photocatalysts and other layered systems.

2. Experimental description

All chemicals were purchased from Sigma-Aldrich. Titanium chloride (TiCl_4 , 99.9%), ethyl acetate ($\text{C}_4\text{H}_8\text{O}_2$, 99%) and *tert*-butylamine ($\text{C}_4\text{H}_{11}\text{N}$, 99.5%) were used as titanium, oxygen and nitrogen sources, respectively.

The CVD reactor

All the components of the CVD apparatus were kept at high temperature (200 °C). The precursors were heated independently in stainless steel bubblers in order to generate enough vapour pressure to be carried into the reactor. Pre-heated nitrogen (supplied by BOC) was used as carrier gas. The precursors were mixed in stainless steel chambers at 250 °C under controlled flow rates and then plain nitrogen flow dragged the mixture of gas precursors through a triple baffle manifold producing a wide laminar flow into the reactor. The CVD reactor was a 320 mm-long heated graphite block with three inserted Whatman heater cartridges. The carbon block was contained in a quartz tube and the temperature controlled using Pt–Rh thermocouples.

In a typical deposition, titanium chloride (TiCl_4) and ethyl acetate ($\text{C}_4\text{H}_8\text{O}_2$) were used as titanium and oxygen sources, respectively. The experimental conditions set for titanium and oxygen precursors were constant in the deposition of all undoped and doped TiO_2 films, with bubblers temperatures of 340 and 310 K and mass flow rates of 6.7×10^{-3} and 3.1×10^{-3} g min^{-1} , respectively. The film growth of the resulting undoped TiO_2 films was *ca.* 350 nm min^{-1} (Table 1). All films were deposited at 500 °C on float glass substrates ($89 \times 225 \times 4$ mm) supplied by the Pilkington NSG Group, which is pre-coated with a SiO_2 barrier layer by the company in order to prevent ion diffusion into the film. The glass substrates were thoroughly cleaned using acetone (99%), isopropanol (99.9%) and distilled water and dried in air prior to use. Details of the particular experimental conditions for the synthesis of the films investigated in this work are given below.

Analytical methods

X-ray diffraction (XRD) analysis was performed using a Bruker-Axs D8 (GADDS) diffractometer. The instrument operates with a Cu X-ray source, monochromated ($K\alpha_1$ and $K\alpha_2$) and a 2D area X-ray detector with a resolution of 0.01°. Films were analysed with a glancing incident angle (θ) of 5°. The diffraction patterns obtained were compared with database standards. UV/Vis spectroscopy was performed using a double monochromated Perkin Elmer Lambda 950 UV/Vis/NIR spectrophotometer in the 300–1000 nm range. Reflectance spectra was recorded for different positions in the range 300–2500 nm on a Helios double beam instrument standardised relative to a silicon mirror, which allowed the thickness of the films to be determined *via* the Swanepoel method.²⁶ The latter measurements were confirmed for selected samples using side-view scanning electron microscopy (SEM). The SEM studies were carried out using a JEOL 6301 (5 kV) and a JEOL JSM-6700F field emission instruments and the Oxford software INCA. X-Ray photoelectron spectroscopy (XPS) was performed using a Thermo K alpha spectrometer with monochromated Al K alpha radiation, a dual beam charge compensation system and constant pass energy of 50 eV. Survey scans were collected in the range of 0–1200 eV. High-resolution peaks were used for the principal peaks of Ti (2p), O (1s), N (1s), C (1s) and Si (2p). The peaks were modelled using sensitivity factors to calculate the film composition. The area underneath these bands is an indication of the concentration of element within the region of analysis (spot size 400 μm).

Photocatalytic test

The photocatalytic performance of the films synthesised in this work was evaluated during photodegradation of octadecanoic (stearic) acid (95%, Sigma-Aldrich). A Perkin Elmer RX-I Fourier transform infrared (FTIR) spectrometer was used to monitor the degradation of stearic acid under UVA illumination. Black light blue (BLB) lamps (Vilber-Lourmat, 2×8 W, 365 nm, 1.2 mW cm^{-2}) were used for the photocatalytic tests. In addition, regular indoor-light (fluorescent) lamps (GE lighting 2D fluorescent GR10q-835 white, 28 W) were used to test the activity of the films in the visible range.

Table 1 Film description and experimental details for the deposition of undoped and N-doped TiO_2 thin-films. The temperature and mass flow conditions were constant for metal (TiCl_4) and oxygen ($\text{C}_4\text{H}_8\text{O}_2$) precursors: 340 and 310 K and 6.7×10^{-3} and 3.1×10^{-3} g min^{-1} , respectively

Sample	Sample description	N mass flow ($\times 10^{-3}$) (g min^{-1})	Deposition time (s)	Film growth (nm min^{-1})	Total N content (at.%)
Ti1	Undoped	—	60	305	—
Ti2	Undoped	—	120	355	—
N1	Non-stratified doped	5.9	60	265	2.0
N2	Non-stratified doped	1.0	120	340	0.25
SL	Single-layer doped	1.3	60/30 ^a	390	0.60
ML	Multi-layer doped	1.3	120/25 ^a	330	0.65

^a Fraction of total time for nitrogen precursor delivery.

3. Results and discussion

Synthesis of stratified nitrogen-doped films

The deposition of nitrogen-doped TiO₂ films (N-TiO₂) was carried out controlling the high vapour pressure of the nitrogen precursor (C₄H₁₁N) by cooling down the bubbler to 275 K using a dry ice bath. The film growth of N-TiO₂ films typically ranged between 300–340 nm min⁻¹, depending on the nitrogen precursor flow rates as determined from side-on SEM. A pulsed delivery of the nitrogen precursor was set so that highly doped regions were intercalated with undoped regions in the deposition of stratified films. Three-dimensional XPS images of the N 1s environment of doped N-TiO₂ films are shown in Fig. 1. The yellow areas in the images indicate highly doped regions in the films. In the case of non-stratified films, the nitrogen precursor was allowed to flow during the entire deposition time (Fig. 1(a)). A single-layer stratified film (SL) was synthesised by allowing the introduction of nitrogen during half the time of total deposition (30 s) (Fig. 1(b)) and the same process was followed in 5 s intervals for the production of a multi-layer stratified N-TiO₂ film (Fig. 1(c)). The corresponding flow rates and deposition conditions are listed in Table 1.

The undoped TiO₂ films deposited were colourless and transparent (Fig. 2, inset), showing interference fringes due to thickness gradients across the samples. In contrast, the N-TiO₂ films were yellow (Fig. 2, inset) and their corresponding absorption spectra showed a red-shift of the absorption edge compared to undoped TiO₂ films (Fig. 2). This shift was not significant in the case of single-layer N-TiO₂ films compared to undoped samples, both types showing threshold wavelengths in the range of 375–385 nm (3.2–3.3 eV), nevertheless, highly doped samples showed important shifts toward the visible range and two optical absorption thresholds were apparent near 460 and 570 nm (2.7 and 2.2 eV), respectively. It is worth noting that no difference was found between comparable non-stratified and stratified N-TiO₂ films in terms of their absorption properties and also that these estimations ignore the scattering component in the spectra. Similar changes have been reported in the incorporation of nitrogen into TiO₂ materials in the literature,¹⁷ however, correlation of these absorption features

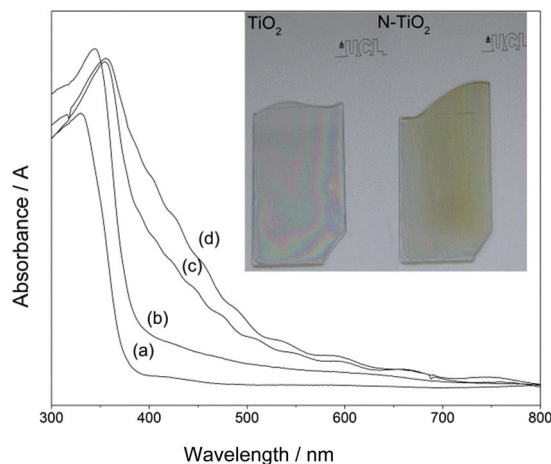


Fig. 2 UV/Vis spectra of typical undoped (a) and N-TiO₂ thin-films: (b) single-layer (SL), (c) non-stratified (N2) and (d) multi-layer (ML) films using *tert*-butylamine as nitrogen source. The inset shows photographs of typical undoped TiO₂ and N-TiO₂ films synthesised by CVD.

and the potential activity of N-TiO₂ materials is a matter of historic controversy.²⁷

All undoped and N-doped films investigated in this work had similar surface morphologies and cross-sectional growth (Fig. 3). SEM analysis showed large star-shaped aggregated particles apparently unaffected by nitrogen doping. However, the incorporation of high concentrations of nitrogen had an impact on the crystallinity of the N-TiO₂ films, as evidenced by XRD analysis (Fig. 4(a)). The broadening and decrease of the anatase diffraction peaks was clearly observed when comparing undoped and doped films of similar thickness. This is in agreement with similar observations reported in the literature.^{1,21,28} In contrast, XRD studies of stratified films containing selected regions of comparable nitrogen concentration showed intense, sharp peaks (Fig. 4(c)), suggesting that their overall crystallinity was largely unaffected by the high doping levels.

The corresponding XPS patterns averaged from a similar thickness range of these films (*ca.* 50 nm) are shown in Fig. 4(b and d). The concentration of nitrogen was estimated from integration of the area underneath each XPS curve in the N 1s environment (397–400 eV). These spectra include one highly doped layer in the case of the stratified ML film. It can be clearly observed that the nitrogen levels within selective regions of

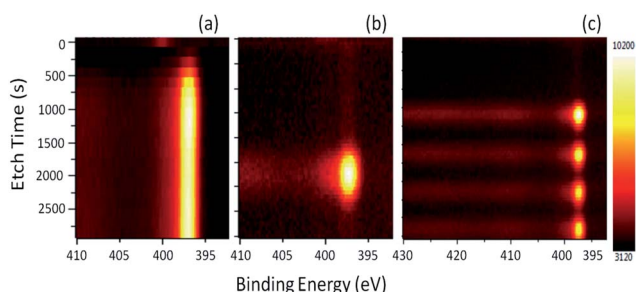


Fig. 1 X-ray photoemission three-dimensional view of the N 1s environment from depth analysis of selected N-TiO₂ thin-films: (a) non-stratified, (b) single-layer stratified and (c) multi-layer stratified doped films. The yellow areas indicate regions of high nitrogen concentration. The main peak in the N 1s environment has been assigned to substitutional nitrogen species (397 eV).

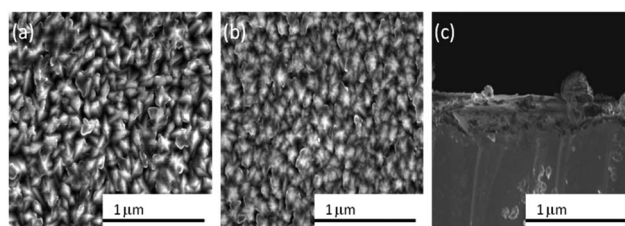


Fig. 3 Scanning electron microscopy (SEM) images of typical (a) undoped and (b) stratified N-TiO₂ films. (c) Side-view SEM of the multi-layer ML N-TiO₂ film.

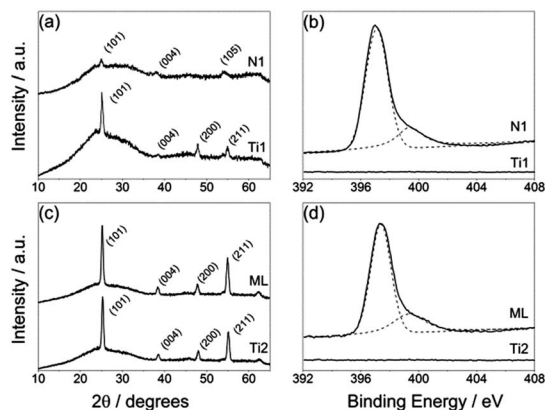


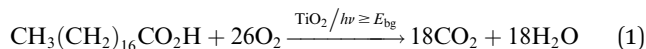
Fig. 4 X-ray diffraction (XRD) and corresponding photoelectron spectra (XPS) of non-stratified, N1 (top row) and stratified, ML (bottom row) N-TiO₂ films containing highly doped regions. The XPS spectra shown here were obtained from averaging data within ca. 50 nm. Patterns of similar undoped (Ti1, Ti2) TiO₂ films have been included for reference.

both films were comparable, 0.70 and 0.50, for N1 (non-stratified) and ML (stratified) samples, respectively.

The strategy of pulsed precursor delivery offered an opportunity to study the effect of a stratified arrangement of highly doped regions in otherwise similar N-TiO₂ films in terms of physical properties.

Photoactivity of stratified vs. non-stratified films

The photocatalytic activity of these films was evaluated upon degradation of a model organic pollutant, octadecanoic (stearic) acid, under UVA irradiation (1.2 mW cm⁻²). The overall degradation reaction is given by eqn (1).



The films were coated with a thin layer of stearic acid using an in house built dip-coater from a 0.05 M stearic acid solution in chloroform. A typical photoactivity test monitoring the photodegradation of stearic acid on a TiO₂ film is shown in Fig. 5(a). The integrated areas of characteristic C–H infrared bands at 2958, 2923 and 2853 cm⁻¹ were calculated upon illumination time (Fig. 5(b)). The photoactivity rates were estimated from linear regression of the initial 40–50% degradation steps (zero-order kinetics). An estimation of the number of molecules of stearic acid degraded on the film was carried out using a conversion factor, considering that 1 cm⁻¹ of integrated area correspond to 9.7×10^{15} molecules of stearic acid.²⁹ Formal quantum efficiencies (FQE), defined as molecules of acid degraded per incident photon (units, molec. photon⁻¹) were calculated assuming all incident photons had the same energy (3.4 eV) and were absorbed by the films.

The formal quantum efficiencies of selected undoped (Ti1, Ti2), non-stratified (N1, N2) and single- (SL) and multi-layer (ML) stratified N-TiO₂ films during degradation of stearic acid under UVA irradiation are shown in Fig. 5(c). As inferred above,

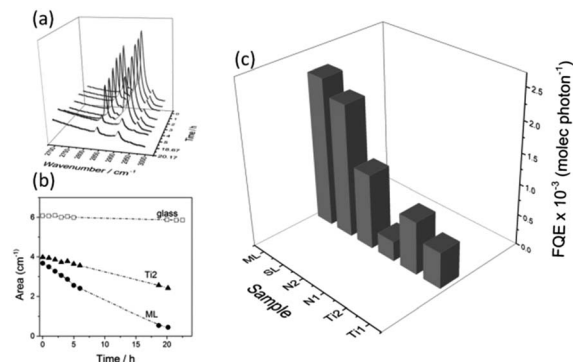


Fig. 5 (A) Infrared spectra showing the photodegradation of stearic acid upon UVA irradiation (1.2 mW cm⁻²) on a multi-layer (ML) stratified N-TiO₂ film. (B) Integrated areas of stearic acid obtained during illumination of undoped, Ti2 (full triangles) and ML stratified films (full circles). The corresponding areas on plain glass (empty squares) have been included for reference. (C) Formal quantum efficiencies, estimated as molecules degraded per incident photon, of selected undoped (Ti1, Ti2), non-stratified (N1, N2) and stratified doped (SL, ML) TiO₂ films.

the poor crystallinity of highly doped non-stratified samples (N1) limited their photocatalytic activity. In contrast, the activity of non-stratified N-TiO₂ films with low nitrogen content (N2) was always enhanced compared to that of similar undoped samples (Ti2) and even higher activities were found in the case of stratified samples (SL, ML), particularly for multi-layer N-TiO₂ films. From merely a structural viewpoint, this is surprising because highly doped regions in stratified films may also be highly disordered areas, which would presumably promote charge carrier recombination and thus diminish their photoactivity. It is worth noting that the XRD patterns of these samples were comparable (Fig. 6(a)) and therefore highly disordered areas would be expected to be very narrow (within short range order), if present at all. Instead, the photocatalytic activities observed were consistent with the total amount of

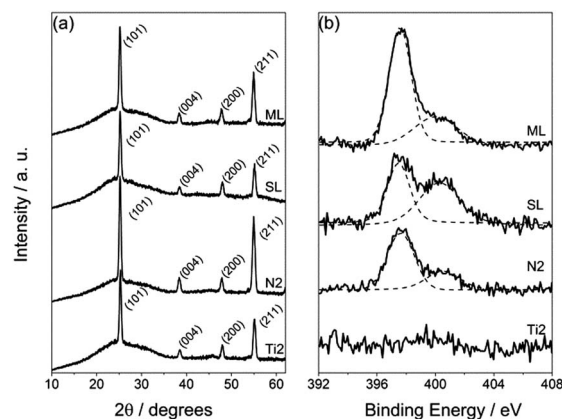


Fig. 6 X-ray diffraction (XRD) and corresponding photoelectron spectra (XPS) of non-stratified (N2), single-layer (SL) and multi-layer (ML) stratified N-TiO₂ films. The XPS spectra were averaged from depth-profile analysis of the entire films. Patterns of a similar undoped (Ti2) TiO₂ film have been included for reference.

nitrogen in the samples, suggesting that there is likely a direct correlation of the nature and concentration of N species in the films and their photoactivities.

The influence of N species on the photocatalytic activity of N-TiO₂ materials is a matter of great controversy in the literature.²⁷ Nitrogen may be incorporated in substitutional (β -N, oxygen lattice site) and interstitial (γ -N) environments into the TiO₂ structure, with corresponding binding energies of 397 and 399–400 eV.^{15,30,31} The specific influence of β - and γ -N species on the photoactivity of N-TiO₂ compounds has been extensively discussed,^{14,32,33} however, no agreement has been reached in this regard. In our case, the photocatalytic behaviour of our samples in the UV range (Fig. 5(c)) did not follow a particular trend for either β - or γ -N species. The content of substitutional nitrogen (β -N, 397 eV) in the multi-layer ML sample was very high compared to those in single-layer SL and non-stratified N2 films (Fig. 6(b)), which could explain the peak activity of the former. However, the β -N concentration in both SL and N2 samples is very similar, in contrast to their corresponding activities. On the other hand, the levels of interstitial nitrogen species (γ -N, 400 eV) were comparable in both ML and N2 samples and only slightly higher in the single-layer SL film (Fig. 6(b)).

Some authors have also reported the role of nitrogen adsorbed species in the efficiency of N-TiO₂ photocatalysts and it is not clear if a synergistic interaction among bulk and adsorbed species is required for the best performance of these materials.²⁰ In our work, XPS analysis of the N 1s environment on the surface showed a peak at 400 eV, which has been commonly assigned to surface adsorbed nitrogen species (γ -N₂, NO_x, NH_x).²⁷ The amount and nature of these surface adsorbed nitrogen species were also comparable among our films and no trace of other nitrogen-containing species (N⁻, NO₃⁻, etc.) was detected.

In addition, other authors^{27,34,35} have highlighted the potential role of oxygen vacancies (V_Os), particularly focusing on their visible activity, which are inherently generated in the incorporation of N³⁻ anions into the TiO₂ structure (intrinsic defects) and also formed under the reductive conditions typically used during nitrogen doping. According to these authors, the photoactivity of N-TiO₂ materials in the visible range correlates with an optimal number of V_Os, above which V_Os would act as carrier recombination centres. Further photocatalytic studies were carried out in the visible range using regular indoor fluorescent lamps, however, no activity was observed beyond instrumental error for any of the films used in the discussion of this work.

The implication for a direct correlation between photoactivity and total concentration of nitrogen in the films is important, admitting that the stratified N-rich regions could act as buffer layers²⁴ that favour the generation of charge carriers. In this case, a valid explanation for the unexpectedly high activity of the stratified films may be proposed in terms of mobility of photogenerated charge carriers. The stratified film is then engineered to contain a combination of N-doped layers, for an increased production of charge carriers, and undoped regions of high mobility, band like-conduction behaviour,³⁶ for

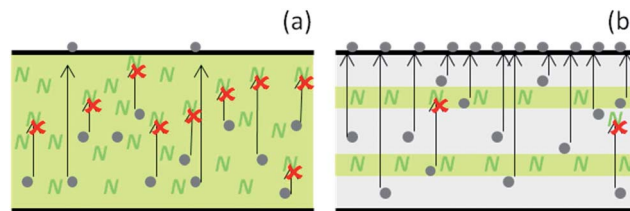


Fig. 7 Schematic figure representing the potential charge carrier mobility and recombination suggested for (a) non-stratified and (b) stratified N-TiO₂ films.

an optimum photocatalytic performance (Fig. 7). In contrast, high nitrogen densities present across the entire non-stratified film could act as carrier recombination centres,³⁵ having a detrimental impact to their photoactivity.

4. Conclusions

A new strategy to synthesise stratified doped TiO₂ films using atmospheric-pressure chemical vapour deposition (APCVD) has been presented. This is to our knowledge the first example of APCVD to be used in pulsed precursor delivery. High concentrations of nitrogen were selectively incorporated during the deposition of TiO₂ anatase films with minor detriment of their overall crystallinity, as suggested by XRD studies. The photocatalytic activity of the resulting stratified films was investigated during degradation of stearic acid. The activity of these films was dramatically enhanced compared to similar non-stratified and undoped films. A possible explanation for this enhancement has been proposed in terms of the combined effects of high charge carrier photo-generation and high mobility, low carrier recombination within highly doped and undoped regions of the stratified films.

Examples of advanced catalyst design such as the one presented in this work urge to a revision of the widely-studied photocatalytic systems for an optimum combination of their physicochemical properties. The selective addition of appropriate amounts of a particular dopant (or mixture of co-dopants) adds yet another variable to the complexity of these systems. The simple strategy employed here for the incorporation of controlled concentrations of nitrogen into TiO₂ films can be used to produce materials with multiple layers using a limited range of dopants. In this sense, the approach is similar to that used in atomic layer deposition and it allows configuration of multi-layer stratified films for the best advantage of carrier generation and mobility.

Acknowledgements

European Commission FP7 is thanked for funding (PCATDES, Grant no. 309846). Dr Robert Palgrave is thanked for his assistance in the XPS analysis. Mr Kevin Reeves and Dr Steven Firth are also thanked for access and assistance to the SEM instruments.

Notes and references

- 1 C. W. H. Dunnill, Z. A. Aiken, J. Pratten, M. Wilson, D. J. Morgan and I. P. Parkin, *J. Photochem. Photobiol., A*, 2009, **207**, 244–253.
- 2 K. Page, R. G. Palgrave, I. P. Parkin, M. Wilson, S. L. P. Savin and A. V. Chadwick, *J. Mater. Chem.*, 2007, **17**, 95–104.
- 3 A. Kafizas, S. Kellici, J. A. Darr and I. P. Parkin, *J. Photochem. Photobiol., A*, 2009, **204**, 183–190.
- 4 A. Mills and S. L. Hunte, *J. Photochem. Photobiol., A*, 2000, **108**, 1–35.
- 5 A. Fujishima, X. Zhang and D. Tryk, *Surf. Sci. Rep.*, 2008, **63**, 515–582.
- 6 E. Hao, B. Yang, J. Zhang, X. Zhang, J. Sun and J. Shen, *J. Phys. Chem.*, 1998, **8**, 1327–1328.
- 7 I. Robel, V. Subramanian, M. Kuno and P. Kamat, *J. Am. Chem. Soc.*, 2006, **128**, 2385–2393.
- 8 Y. Maeda, S. Kimura, M. Kanda, Y. Hirashima, T. Hasegawa, T. Wakahara, Y. Lian, T. Nakahodo, T. Tsuchiya, T. Akasaka, J. Lu, X. Zhang, Z. Gao, Y. Yu, S. Nagase, S. Kazaoui, N. Minami, T. Shimizu, T. Tokumoto and R. Saito, *J. Am. Chem. Soc.*, 2005, **127**, 10287–10290.
- 9 D. E. Wynkoop, *Environ. Sci. Technol.*, 1996, **30**, 1660–1666.
- 10 M. Ni, M. K. H. Leung, D. Y. C. Leung and K. Sumathy, *Renewable Sustainable Energy Rev.*, 2007, **11**, 401–425.
- 11 M. Litter, *Appl. Catal., B*, 1999, **23**, 89–114.
- 12 A. Fujishima and X. Zhang, *C. R. Chim.*, 2006, **9**, 750–760.
- 13 G. Wu, T. Nishikawa, B. Ohtani and A. Chen, *Chem. Mater.*, 2007, **19**, 4530–4537.
- 14 A. Zaleska, *Recent Pat. Eng.*, 2008, **2**, 157–164.
- 15 R. Asahi, T. Morikawa, T. Ohwaki, K. Aoki and Y. Taga, *Science*, 2001, **293**, 269–271.
- 16 A. Mills, M. Crow, J. Wang, I. P. Parkin and N. Boscher, *J. Phys. Chem. C*, 2007, **111**, 5520–5525.
- 17 K. S. Han, J. W. Lee, Y. M. Kang, J. Y. Lee and J. K. Kang, *Small*, 2008, **4**, 1682–1686.
- 18 J. Cao, Y. Zhang, H. Tong, P. Li, T. Kako and J. Ye, *Chem. Commun.*, 2012, **48**, 8649–8651.
- 19 J. Cao, Y. Zhang, L. Liu and J. Ye, *Chem. Commun.*, 2013, **49**, 3440–3442.
- 20 J. Tao, M. Yang, J. W. Chai, J. S. Pan, Y. P. Feng and S. J. Wang, *J. Phys. Chem. C*, 2014, **118**, 994–1000.
- 21 H. M. Yates, M. G. Nolan, D. W. Sheel and M. E. Pemble, *J. Photochem. Photobiol., A*, 2006, **179**, 213–223.
- 22 Y. S. Jung, A. S. Cavanagh, L. A. Riley, S. H. Kang, A. C. Dillon, M. D. Groner, S. M. George and S. H. Lee, *Adv. Mater.*, 2010, **22**, 2172–2176.
- 23 L. Li, G. S. Rohrer and P. A. Salvador, *J. Am. Ceram. Soc.*, 2012, **95**, 1414–1420.
- 24 H. O. Seo, S. Y. Park, W. H. Shim, K. D. Kim, K. H. Lee, M. Y. Jo, J. H. Kim, E. Lee, D. W. Kim, Y. D. Kim and D. C. Lim, *J. Phys. Chem. C*, 2011, **115**, 21517–21520.
- 25 W. H. Shim, S. Y. Park, M. Y. Park, H. O. Seo, K. D. Kim, Y. T. Kim, Y. D. Kim, J. W. Kang, K. H. Lee, Y. Jeong, Y. D. Kim and D. C. Lim, *Adv. Mater.*, 2011, **23**, 519–522.
- 26 R. Swanepoel, *J. Phys. E: Sci. Instrum.*, 1983, **16**, 1214–1222.
- 27 A. V. Emeline, V. N. Kuznetsov, V. K. Rybchuk and N. Serpone, *Int. J. Photoenergy*, 2008, **2008**, 1–19.
- 28 T. Okato, T. Sakano and M. Obara, *Phys. Rev. B: Condens. Matter Mater. Phys.*, 2005, **72**, 115–124.
- 29 A. Mills, J. Wang and D. Ollis, *J. Catal.*, 2006, **243**, 1–6.
- 30 O. Diwald, T. L. Thompson, E. G. Goralski, S. D. Walck and J. T. Yates, *J. Phys. Chem. B*, 2004, **108**, 52–57.
- 31 S. H. Cheung, P. Nachimuthu, M. H. Engelhard, C. M. Wang and S. A. Chambers, *Surf. Sci.*, 2008, **602**, 133–141.
- 32 C. Di Valentin, E. Finazzi, G. Pacchioni, A. Selloni, S. Livraghi, M. C. Paganini and E. Giamello, *Chem. Phys.*, 2007, **339**, 44–56.
- 33 E. Finazzi, A. Selloni, G. Pacchioni and C. Di Valentin, *J. Phys. Chem. C*, 2007, **111**, 9275–9282.
- 34 A. V. Emeline, A. V. Frolov, V. K. Ryabchuk and N. Serpone, *J. Phys. Chem. B*, 2003, **107**, 7109–7119.
- 35 H. Irie, Y. Watanabe and K. Hashimoto, *J. Phys. Chem. B*, 2003, **107**, 5483–5486.
- 36 H. Tang, K. Prasad, R. Sanjinès, P. E. Schmid and F. Lévy, *J. Appl. Phys.*, 1994, **75**, 2042–2047.